Tunable Antenna-Coupled Metal-Oxide-Metal (MOM) Uncooled IR Detector

Pashang Esfandiari (Missile Defense Agency), G. Bernstein, P. Fay, W. Porod, B. Rakos A. Zarandy (EUTECUS/University of Notre Dame), B. Berland, L. Boloni, G. Boreman, B Lail, B. Monacelli, A. Weeks (ITN/University of Central Florida)

1.0 Abstract

Missile Defense Agency/Advanced Systems, in partnership with both EUTECUS/University of Notre Dame (UND) and ITN Energy Systems/University of Central Florida (UCF) has embarked on developing a multispectral imaging IR sensor. This technology, when matured, could revolutionize IR sensor technology by reducing the need for cooling, eliminating lattice matching and avoiding epitaxial fabrication processes. This paper describes the approaches employed by both EUTECUS/UND and ITN/UCF teams to integrate nano-antenna technology with the existing cellular neural network (CNN) processor to produce multispectral IR sensors. This effort is a leap into the performance realm where biological systems operate.

2.0 Introduction

In missile defense, there is a need for sensors that are lightweight, use low-power and have reduced complexity. The antenna-based IR detectors seem to fit these criteria and offer a new direction in multispectral sensing with many advantages over other imaging techniques. The nano-antenna coupled MOM detectors are easier to fabricate, have no need for cryo-cooling and are low noise devices that operate at room temperatures. These sensors have no moving parts and are made of solid state nano-electronics that use a small amount of power for operation. The MOM detectors have been used as mixers in heterodyne detection and because of their fast response time, they have been extensively used in absolute frequency measurement for the development of time and frequency standards [1]. The small size, low power and their inherent compatibility with standard silicon processing makes it possible to integrate them directly with processing circuitry. This allows a seamless merging of sensor and processing elements, and thus offers the possibility of integrated light-weight and low-power systems.

The goal of the Missile Defense Agency (MDA) is to build an integrated layered missile defense system to defend against all ballistic missile threats during all phases of the trajectory. A notional trajectory of a ballistic missile can be divided into three phases: the boost, the midcourse and the terminal phase. Each phase is to be defended by at least two weapon systems. Currently, the boost phase is expected to be defended by Kinetic Energy Interceptors (KEI) and an Airborne Laser (ABL). The midcourse is defended by Ground-based Missile Defense (GMD) and sea-based midcourse (Aegis Ballistic Missile Defense). The terminal phase is to be defended by the existing Terminal High Altitude Air Defense (THAAD) and advanced PATRIOT (PAC-3). Collectively, these weapon systems are referred to as the Ballistic Missile Defense System (BMDS). The effective operation and evolution of the BMDS relies on a number of matured and diverse technologies that support propulsion; guidance and navigation; a host of sensors (surface, air and space); and Command, Control, Battle Management and Communications (C2BMC).

In general, a BMDS interceptor is composed of a booster and a kill vehicle (KV). The function of the booster is to deploy the KV into a proper endo- or exo-atmospheric region (acquisition basket) where it has the best possible opportunity to acquire the target. The KV includes a propulsion sub-system, a guidance and navigation unit, a seeker (passive or active sensor or a combination of the two), plus the mission and seeker processors and the supporting electronics. During its flight toward the target, the KV is provided periodic target updates by surface-based radar and C2BMC for fire control solutions. Based on the provided information and its own seeker information, the KV acquires and tracks the designated target (Reentry Vehicle, RV). During its flight, the KV propulsion continually keeps the KV on course to intercept the RV. The KV uses its kinetic energy to hit and destroy the incoming RV.

One of the most challenging KV functions is target/decoy discrimination. During the midcourse portion, the incoming RV may deploy decoys and shed flight debris. The KV seeker must be able to discriminate among these objects and

Infrared Technology and Applications XXXI, edited by Bjørn F. Andresen, Gabor F. Fulop, Proc. of SPIE Vol. 5783 (SPIE, Bellingham, WA, 2005)
0277-786X/05/$15 · doi: 10.1117/12.606874

identify the RV in real-time and keep the KV on an intercept path with the RV. Since the size, mass and power associated with KV homing sensor(s) and the supporting hardware/software subsystems are the principal determinant of the overall size, mass and power needs of the KV, a KV with reduced mass, power and cooling requirements can offer profound advantages. One common goal for interceptor based BMDS elements is miniaturization of the KV. To this end, MDA scientists and engineers, along with their industry partners, have long identified the inter-relationship between mass and time in missile defense as an area that is ripe for the infusion of revolutionary technologies. The mass and power reductions and system efficiencies gained in these two critical parameters will provide significant improvements in the overall missile interceptors' (KVs) design and performance.

The advent of nano-electronics and lightweight high-throughput computing machines could have a major impact on KV sensing and computing functions. This paper addresses the development of antenna-coupled MOM detectors. Future work will address the integration of these detectors with CNN processors for the design and development of a multispectral imaging IR sensor.

The CNN is a unique ultra high-speed sensor-processor. It is a mix of analog and digital components with the latest array size of 128 x 128. What makes the CNN a unique sensor-processor is the fact that each sensor in the array is locally integrated with its computing, storing and communication units. This integration of the sensor and the processor has reduced the I/O delay substantially. Currently, the sensing elements in CNN are photodetectors operating in the visible region at very high frame rates (upward of thousands of frames per second). In this effort, the photodetector are to be replaced by antenna-based IR sensors.

3. Antenna-Coupled MOM Detectors

Antenna-based MOM sensors consist of two key elements: (1) An antenna to efficiently couple to incident electromagnetic radiation, and (2) a high frequency MOM diode that rectifies the AC signal from the antenna, generating a DC signal to external readout circuitry. Figure 1 shows a scanning electron microscope image of an antenna coupled MOM IR detector. The thin film MOM, fabricated at the feed points of a nano-antenna, consists of an oxide layer sandwiched between two metal electrodes. An array of IR detectors is fabricated on an insulating substrate using standard lithographic techniques. To achieve the fine feature sizes (sub 100 nm), direct-write electron-beam lithography is employed. Various metals and their oxides have been used for MOM diode-antenna combination. Figure 1 shows two nickel antenna arms sandwiching a nickel oxide layer.

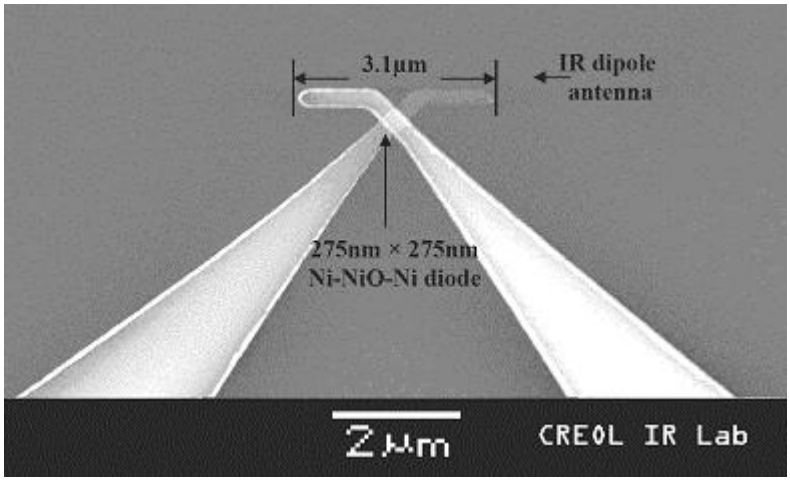

Figure 1 – Scanning-electron micrograph of an infrared antenna-coupled MOM diode. The oxide layer is sandwiched between the two arms of the antenna.

4. Benefit of Antenna-Coupled Detectors

The key advantage of the antenna-based detector approach is that the antenna-based detectors offer inherent frequency agility and polarization sensitivity without the need for bulky and expensive filters that are required in standard bolometric FPA designs. The antenna-based sensor approach exclusively utilizes electronic processes for IR detection, as opposed to heating of bolometers. Electronic processes (such as quantum mechanical tunneling) inherently are much faster than thermal processes, and are expected to translate into faster detector response. In addition to faster response times, the wave-phenomena-based antenna also offers frequency selectivity through the physical length of the antenna arms (resonance effect due to standing waves). In contrast thermal processes do not exhibit strong frequency dependence.

5. Activities and Accomplishments of Team members

To explore the issues and the challenges associated with the integration of the nano-antennas with CNN, MDA/Advanced Systems provided small business technology transfer (STTR) Phase I funding to two teams. These teams have agreed to pursue the feasibility of combining the sensing and computing technologies, namely the integration of the nano-antennas operating in IR with a CNN processor capable of imaging a scene at a very high frame rate. The selected teams are EUTECUS/UND and ITN Energy Systems, Inc./UCF. This effort was divided into two phases: In Phase I, the teams were to:

a) Design a multispectral IR imager based on nano-antenna-coupled MOM detectors
b) Use modeling and measurement to demonstrate antenna-coupled MOM detector performance
c) Develop interface control protocols and documentation to enable integration of the MOM detectors with an 8x8 CNN chip

6. MOM Background

The operation of metal-oxide-metal (MOM) diodes, also known as metal-insulator-metal (MIM) or metal-barrier-metal (MBM) diodes, combined with antennas is based on the rectification of the high-frequency antenna currents induced by the incident radiation. Since high quality infrared imaging systems require fast and sensitive detectors, which are selective to certain frequencies, these sensors are very promising. Unlike semiconductor-based infrared detectors, these devices can operate at room temperature. Although micro-bolometers can also operate at room temperature, they are much slower than the antenna-diode structures.

Point-contact MOM diodes combined with wire antennas were first used for the detection and mixing at sub-millimeter wavelengths in 1966 [2]. In the following years, these structures were applied to detect IR radiation [3], [4], and visible light [5]. Point-contact devices are not suitable for commercial applications because of their mechanical instability and noneproducibility. With the application of photolithography it is now possible to integrate stable and reproducible thin-film Ni-NiO-Ni diode-antenna structures onto a substrate [6]. Although the antenna was not suited for the 10.6 micron radiation, these devices gave significant rectified signals at that wavelength. Electron beam lithography made it possible to fabricate diodes with very small contact areas (around 110 nm x 110 nm) combined with antennas suited for the 10.6 μm radiation [7], 8], [9]. Since a diode with a smaller contact area has a higher cutoff frequency, these devices have a better performance than the structures made by photolithography.

The Notre Dame group has developed a fabrication procedure for dipole antenna-coupled MOM diodes with ultrasmall contact areas (around 50 nm x 50 nm) suited for the detection of 10.6 μm infrared radiation. Both symmetrical and asymmetrical diodes were fabricated using a one-step electron beam lithography followed by a double-angle evaporation. Al-Al_2O_3-Al, Al-Al_2O_3-Ti, Al-Al_2O_3-Pt, Al-Al_2O_3-Ni and Ni-NiO-Pt diodes have been fabricated, and their dc characteristics have been were studied. The asymmetrical MOM diodes are nonlinear even if they are unbiased, and this leads to a lower noise level and thus better performance.

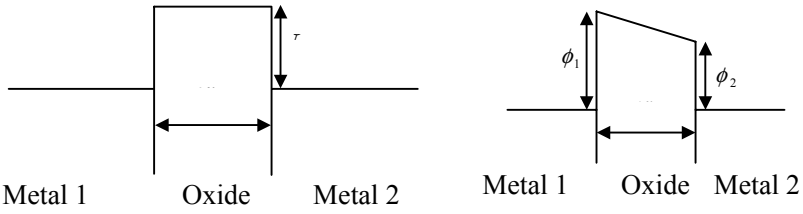

Figure 2. Schematic drawing of symmetrical and asymmetrical MOM

7. Anatomy of MOM detectors

MOM diodes consist of two metal layers separated by an oxide layer. Since the oxide is an insulator, charges can flow from one side to the other either by being sufficiently energetic to overcome the potential barrier (thermionic emission) or by direct "tunneling" through the barrier (quantum mechanical tunneling for sufficiently thin barriers). The energy diagram of a symmetrical and an asymmetrical diode is displayed in Figure 2. Of particular interest here is quantum mechanical tunneling since it is very fast and the nonlinear behavior of the tunneling current-voltage characteristics can be used for the rectification of alternating currents.

The fabrication of MOM diodes for our purposes is rather challenging since the contact area needs to be very small (required small junction capacitance) and the oxide layer has to be very thin in order to yield useful current levels (the tunneling current depends exponentially on the oxide thickness). The Notre Dame group has been working on this challenge in the context of a different problem, namely ultra-small tunnel junctions for single electron transistors. For a junction with a capacitance of atto Farads (10^{-18} F), the transfer of a single electron leads to a change in voltage of 0.16 V, which may be exploited for single-electron device applications. The Notre Dame group now is able to routinely fabricate MOM diode structures with a contact area on the order to 50 nm x 50 nm and oxide thicknesses around 1 or 2 nm.
The ITN/UCF team is working on the tuning aspects of the antenna-coupled MOM diode IR detector, with the focus on the antenna resonance. This technique may result in a multispectral tuning capability.

8. Antenna-Coupled MOM Detectors—Technology Challenges and Risks

The greatest challenge involves achieving sufficient sensitivity comparable to or better than existing IR sensors. A minimum specific detectivity of about $1x10^9$ cm-$Hz^{1/2}$/W is likely required for uncooled imaging applications involving object tracking and discrimination. Many factors affect MOM detector response, including MOM diode performance, antenna design, and coupling efficiencies. Minimization of parasitic diode capacitance and 1/f noise is crucial to achieving high sensitivity for the MOM diodes. High diode nonlinearity, which is a function of MOM materials and fabrication processes, is also critically important. Each of these factors has unique signatures in performance evaluation, and can therefore allow systematic performance optimization.

A moderate risk associated with our sensor design is the successful integration of a single-element antenna onto a tunable substrate. While large-area substrate tuning has been demonstrated, the integration of a single element onto the substrate has not been experimentally verified. The substrate thickness (antenna-to-ground plane separation) is one way of tuning the antenna to its resonant frequencies. By coupling the modeling efforts with the fabrication experience and experimental measurements, an effective tunable antenna-coupled MOM diode detector will be designed and fabricated.

The integration of nano-antenna detectors with CNN chip will also pose challenges. The integration with a CNN chips, fabricated by EUTECUS will be done in Hungary. Compatibility between the two distinct fabrication processes need to be assured. One issue will be the possibility of oxidized metal layers, which might result in parasitic resistances and capacitances.

Another challenge is to extend the tuning range of the tunable antenna-substrate combination to cover the wider range of LWIR. Initial results have been encouraging and at least one micrometer tuning range per antenna element has been

demonstrated. A broad IR band (i.e. 8-12 μm) can be covered with a series of tunable antennas, each responding to a portion of the total band. Therefore, multispectral imaging may be achieved in the near term with a series of discrete elements covering different portions of the LWIR band. This tuning approach will enable sensors to be "programmed" to match various scene conditions, i.e., real-time optimization of the sensor can match source signatures in a scene. Our initial efforts at this tunable design are discussed in the following section.

9. Antenna-Coupled MOM Detector Design

The antenna structures were fabricated on an oxidized, around 625 μm thick, 11-16 Ωcm p-type silicon wafer. The approximately 1.5 μm thick silicon dioxide layers on the top and the bottom of the wafer were grown by wet oxidation for 210 minutes at 2000 °C. The oxide layer acts as an insulator between the devices and the silicon layer, and it serves as a quarter-wave matching layer for the around 10 micron IR radiation [8].

The detector consists of a MOM diode integrated together with a dipole antenna. Detection of the 10.6 μm infrared radiation requires a 3 μm long dipole antenna [8]. The device was fabricated with one-step electron beam lithography combined with double-angle evaporation and oxidation. This process is simple, stable, and permits controlled oxidation, since the sample can be kept in the vacuum chamber. After the deposition of the first metal layer, oxygen can be bled into the chamber at a certain pressure for a certain time, the second evaporation can be done at another angle by tilting the sample stage. Tunnel junctions for the realization of single electron transistors have been fabricated with this method [8].

As schematically shown in Figure 3, during the double-angle evaporation process a metal layer is first deposited though an opening in a two-layer resist mask (in our case at around 7° with respect to normal incidence). Then, this deposited metal structure is oxidized, and another metal layer is deposited at another angle (in our case, -7° with respect to normal incidence). In this way, the pattern is shifted, and the small overlap between the two subsequent metal layers forms the MOM diode. Using this process, it was possible to fabricate diode structures with an overlap area of around 50 nm x 50 nm.

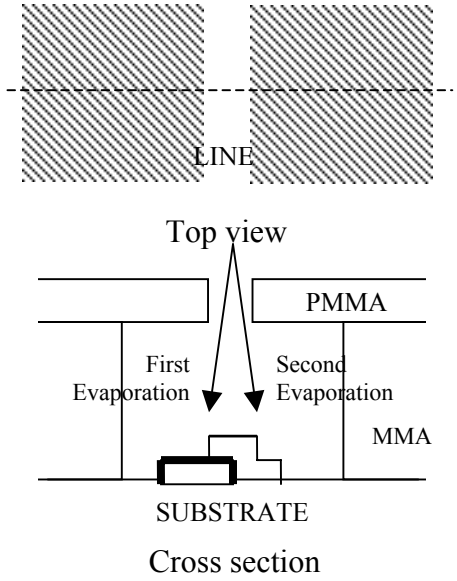

Figure 3. Schematic of the double-angle evaporation process. During the first evaporation step, a metal structure is deposited through the opening in a two-layer resist mask. The oxidation process is indicated by the thick border. Then, a second evaporation step at a different angle creates the MOM structure.

An electron micrograph of a typical antenna-diode structure is shown in the Figure 4. We fabricated Al-Al_2O_3-Al, Al-Al_2O_3-Ti, Al-Al_2O_3-Pt, Al-Al_2O_3-Ni and Ni-NiO-Pt structures with this process. The Al-Al_2O_3-Al diodes were made both with oxidation in air and with oxidation at 60 mTorr for 10 minutes. The Al-Al_2O_3-Ti and Al-Al_2O_3-Pt diodes were fabricated with oxidation in air.

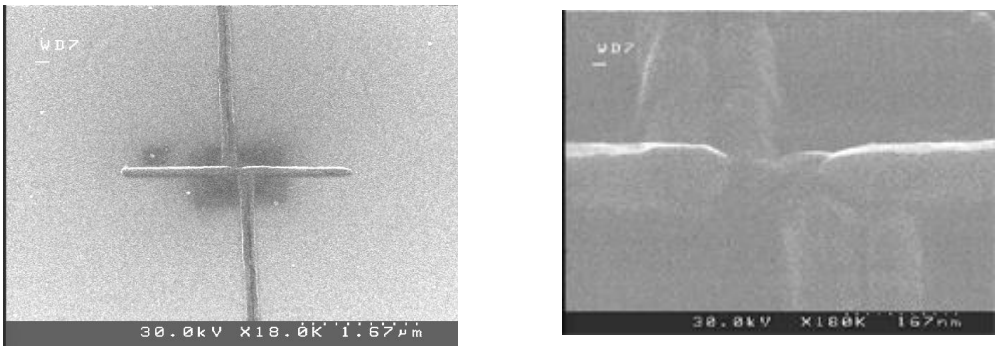

Figure 4. Electron micrograph of an antenna-coupled MOM structure (left image). The right image shows a close-up view of the overlap area in the center, which results from the double-angle evaporation process.

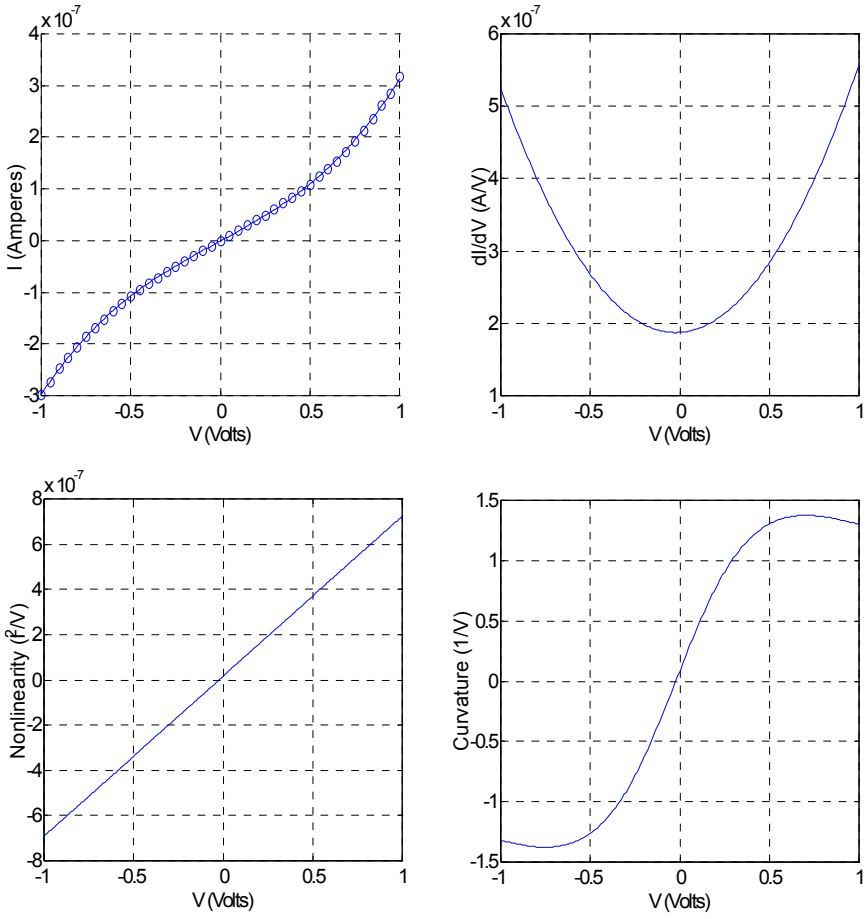

Curvature Coefficient

Figure 5 .I-V characteristic of a typical Al-Al_2O_3-Al diode (upper left), the first derivative (upper right) and second derivative (lower left) of the I-V curve, and the curvature coefficient of the diode (lower right). The circles represent the measured data points, and the continuous curve represents the fitted I-V curve.

10. MOM Diode Current-Voltage Characteristics (I-V Curves)

The current-voltage characteristics of the fabricated diodes were measured at a probe station. The first and second derivatives of the I-V curves were obtained from the curves fitted to the experimental data with a third-order polynomial fit. This data was then used to determine the curvature coefficient. The curvature coefficient γ is the ratio of the second derivative to the first derivative.

Symmetrical Al-Al2O3-Al diodes: These diodes were fabricated with controlled oxidation. After the deposition of the first 30 nm thick Al layer, the aluminum was oxidized at 60 millitorr for 10 minutes, which leads to an approximately 1 nm thick Al_2O_3 layer. The oxidation was followed by the deposition of another 30 nm thick Al layer at another angle. The Al-Al_2O_3-Al devices made with oxidation in air were more stable

than the diodes made with the controlled oxidation. This may be due to the thicker (around 2 nm) oxide layer. The peak curvature coefficients of these diodes were around 1-1.5 V^{-1} (see Figure 5). The zero bias resistance of the diodes is on the order of mega ohms.

Asymmetrical Ni-NiO-Pt diodes: These diodes were made by depositing a 30 nm thick Ni layer, which was then oxidized in air, followed by the deposition of a 30 nm thick Pt layer. We achieved zero-bias curvature coefficients around -3 V^{-1}, and the peak curvature coefficients are around -13 V^{-1} (see Figure 6).

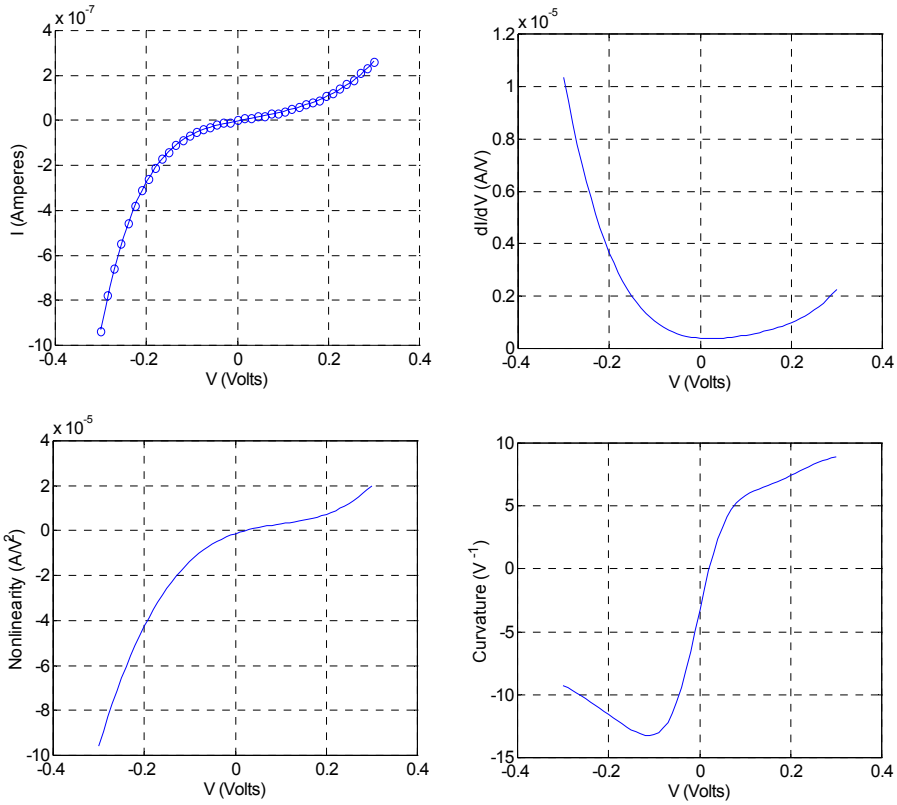

Curvature Coefficient

Figure 6. I-V characteristic of a typical Ni-NiO-Pt diode (upper left), the first derivative (upper right) and second derivative (lower left) of the I-V curve, and the curvature coefficient of the diode (lower right).

Diode	Curvature Coefficient at Zero-Bias (1/V)	Peak Curvature Coefficient (1/V)
Al-Al_2O_3-Al	+ 0.1	-1.4
Al-Al_2O_3-Ti	0.6	2
Al-Al_2O_3-Pt	1	1.3
Al-Al_2O_3-Ni	0.5	1
Ni-NiO-Pt	-3	-13

Table 1. Summarizes the zero-bias curvatures for several asymmetrical MOM diode structures.

11. Figures of Merit Estimates

Several figures of merit are customarily used to describe detector performance and to provide comparisons across different technology platforms. Those which are of most interest in analyzing the performance of uncooled thermal imaging arrays are the responsivity, noise equivalent power, specific detectivity (D*), noise equivalent temperature difference (NETD), minimum resolvable temperature difference (MRTD), and thermal response time. [11-14]. As one example of determining such figures of merit, we calculate in the following steps the specific detectivity, D* ("dee-star") and its associated parameters, based on modeling, measurements and reasonable assumptions.

Definitions:

The specific detectivity is defined by,

$$D^* = (Aeff\ \Delta f)^{1/2} / Pn \qquad (1)$$

where Aeff is the antenna capture area, Δf is the bandwidth, and Pn is the noise equivalent power (NEP) given by

$$Pn = Vn/\beta v \quad . \qquad (2)$$

Here, Vn is the noise voltage across the MOM, and βv is the responsivity. βv is defined as the signal voltage, Vs, divided by the incident radiant power, Po:

$$\beta v = Vs/Po \quad . \qquad (3)$$

For diode-coupled antennas, the responsivity is given by,

$$\beta v = 2 * Zant * \gamma \qquad (4)$$

where Zant is the antenna impedance, and γ is the curvature coefficient of the diode current-voltage characteristics (defined as $\gamma = (d^2I/dV^2)/(dI/dV)$, i.e. the ratio of the second derivative of the diode I-V curve to the first derivative).

We assume that Johnson noise is the dominant noise source, and the noise voltage Vn is given by the well-known expression,

$$Vn = (4\ kT * Rd * \Delta f)^{1/2} \qquad (5)$$

Where, kT is the thermal energy (k is Boltzmann's constant and T is the absolute temperature), Rd is the diode resistance, and Δf is the bandwidth of the system incorporating the detector.

Estimates:

With the above definitions, estimates for the responsivity is provided, noise equivalent power, and specific detectivity for our nanoantenna-coupled MOM diodes.

First, an estimate for the responsivity. For the above definition (4), we take a value for the nanoantenna impedance Zant of 100 ohm, which is derived from our electromagnetic modeling, and we use a value of $\gamma = 13$ 1/V for the curvature coefficient, which is a value obtained from experiment for Ni-NiO-Pt diodes (compare Table 1 above). With these values, the responsivity becomes:

$$\beta v = 2600 \text{ V/W}$$

Next, the estimate the noise voltage at room temperature (T=300K). Based on values reported in the literature, use a value of Rd = 100 ohm for the diode resistance [9]. With this, the noise voltage per unit frequency ($\Delta f = 1$ Hz) becomes:

$$Vn = 1.3\ 10^{-9} \text{ V} \quad .$$

Combining estimates for the noise voltage and the responsivity, the estimate for the noise equivalent power. Using the above definition (2), Pn is estimated to be

$$Pn = 5.0\ 10^{-13} \text{ W} \quad .$$

Using an effective nanoantenna capture area, Aeff, of 10 square microns, based on electromagnetic simulations for our dipoles of length 3 microns. Finally, substituting all values in equation (1), an estimate for D* becomes:

$$D^* = 6 * 10^{8} \text{ cm Hz}^{1/2} \text{/W} \ .$$

This is a respectable value, given the early stage of this technology, but more work is needed to improve D* for antenna-coupled MOM diodes. Improvements are possible through MOM diodes with improved curvature coefficients.

12. Antenna with Tunable Spectral Response

Currently, two approaches are being considered for substrate design to tune the antennas. One design uses static resonance (Figure 7, left) and the other capacitive tuning (Figure 7, right). In either method the objective is to change the thickness of the insulator layer, the layer which separates the antenna from its ground plane. This change in the antenna ground plane influences the antenna resonance. The ability to electrically control the effective ground plane location is verified with a sample of epitaxial silicon on silicon wafer (Figure 7). A sample of silicon wafer with an epitaxial pn-junction is characterized via Infrared Variable–Angle Spectroscopic Ellipsometry on a J.A. Woollam ellipsometer. The thickness and optical parameters of the wafer and epitaxial layer are measured and modeled with the ellipsometer software. In order to apply a voltage uniformly through the substrate, a thin metal layer is deposited atop the epitaxial silicon to act as the upper electrode. This thin film layer is used in place of the antenna bondpad to study the substrate performance. Also, typical antenna bondpad sizes are on the order of hundreds of micrometers, and the optical spot size of the ellipsometer is approximately 3 mm in diameter. The upper electrode layer is also included in the ellipsometer software model.

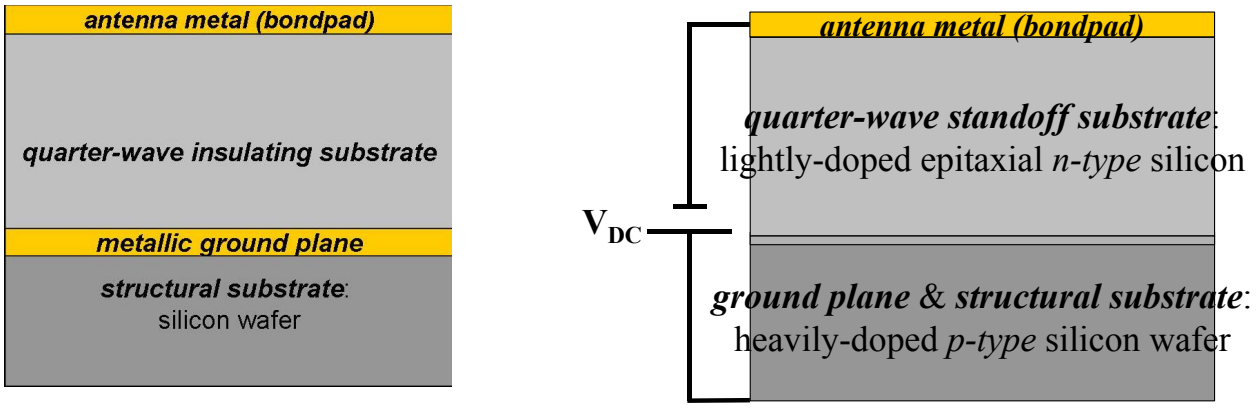

Figure 7 – Comparison of the static-resonance substrate (left) and the tunable-resonance substrate design (right) proposed in this paper.

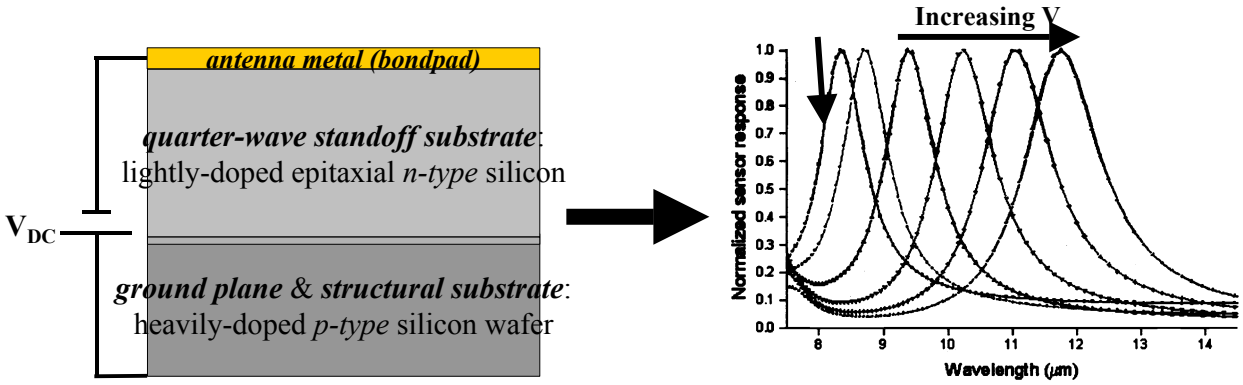

Figure 8. Capacitively-tuned antenna for multi-spectral sensor

As the applied voltage increases, so does the depletion layer thickness demonstrating how the pn-junction can be altered to change the standoff layer thickness and thus, the effective ground plane location. With the increase in applied voltage, the effective thickness of the epitaxial silicon layer in the software model was fit to the measured data. Fig. 9 shows the observed change in the thickness of this layer as function of applied voltage.

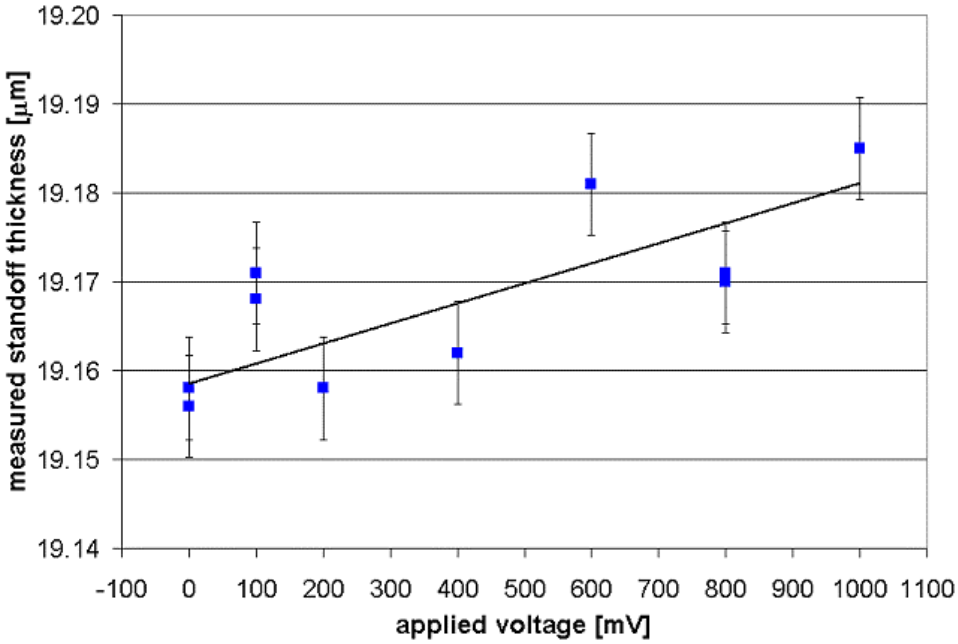

Figure 9 – Demonstration of an applied voltage through the pn-junction substrate and the resulting change of insulating standoff layer thickness.

13. Integration of the MOM Detectors with CNN

To maximize MOM diode detector performance, it is necessary to dc bias each MOM diode for operation in the region of high nonlinearity. The bias level for optimal performance is determined from conventional I-V curve measurements. Typical bias levels for these diodes are on the order of hundreds of millivolts. To regulate the bias voltage, the detector is placed in a voltage divider configuration, as shown in the far-left stage of the circuit schematic of Fig. 10.

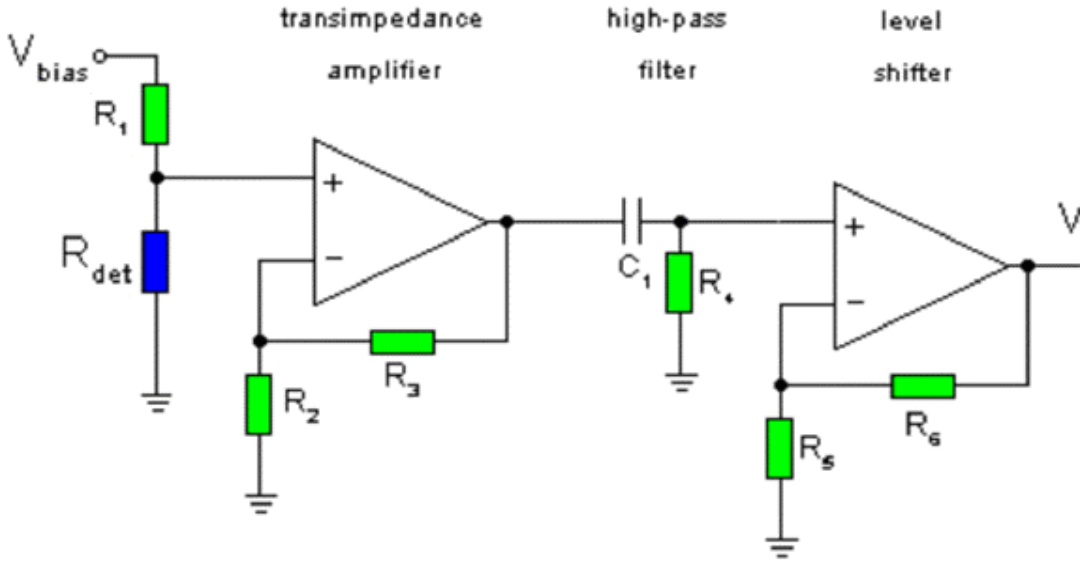

Figure 10 – Low-noise circuitry required to read the signal detected by the antenna-coupled diode.

The output signal of this voltage divider is then sent through a low-noise transimpedance amplifier. Typical amplification factors per stage is 10X to 100X, depending on the well-characterized noise-limiting factors of the system.

Incident radiation is modulated by a mechanical chopper prior to absorption by the antenna. This allows the measurement to be performed in the detector-noise limit, outside of the frequency range dominated by one-over-f and electronics noise. So the detected THz signal, and therefore the rectified dc signal are modulated at the chopper frequency. It is then critical to send the amplified signal through a high-pass filter to separate the modulated detector signal from the dc bias signal. The final stage of the readout circuitry is another amplifier that sets the detector signal to the voltage required by the underlying signal-processing electronics. This voltage is then input directly into the CNN for collection and image processing.

In the first generation imager, the antenna-coupled MOM detector will be connected with the CNN interface via a printed circuit board (PCB). In this case, the antenna-coupled MOM and required signal processing circuitry are input into the CNN channels via patterned wires on the PCB. The MOM signals are processed into a DC voltage that is compatible with the input of the CVM die. A key challenge of our effort is to demonstrate that high frame rates can be achieved with nano-antennas integrated into the CNN. We need to design and develop architectures for direct electrical connection of the nano-antenna sensor with CNN that preserves the high frame rates achieved by CNN

14. Future Plans

The future plans include risk reduction activities in the following areas:

- Increased antenna-based sensor sensitivity to at least or better than the level of current IR sensors
- Improve thin film MOM diode sensor reproducibility processes
- Eliminate parasitic MOMs in the interconnects for integration with an 8 X 8 CNN chip
- Integrate of antenna-based MOM sensor with an 8 X 8 CNN chip
- Demonstrate multispectral sensor functionality (sensing and computing)

15. Summary/Conclusions

Multispectral IR sensors are needed for target detection, discrimination and tracking. With the advances in nano-electronics and its application to multispectral sensor by the two teams, MDA is making strides towards the development of a multispectral sensor prototype. The integration of these two diverse technologies is a leap into a performance realm where biological systems operate. This effort greatly advances the state-of-the-art of the multispectral sensor technology using a novel detection and processing design.

To this end the MDA team has, currently, a design for an uncooled antenna-based multispectral IR detector, signal processing circuitry and defined interface control protocol for direct electrical integration of MOM detectors with a CNN processor chip.

16. Acknowledgement

The authors are grateful to Mr. Gary Payton (Deputy for Advanced Systems, Missile Defense Agency), Col. Larry Strawser and Dr. James Mulroy for their support and continued interest in this effort; Commander Doug Small (Head, Sensor Systems) and Dr. Meimei Tidrow for their encouragement and guidance; Dr. Denise Podolski for her valuable comments on the initial draft; and a special thanks to Dr. Hugo Weichel for the time and effort he devoted to numerous reviews and suggestions that improved this paper. This work has been a team effort and the author wishes to acknowledge the contributions from EUTECUS/University of Notre Dame and ITN/University of Central Florida/MEI. This work was supported by the Missile Defense Agency (STTR Program).

17. References

1. C. Fumeaux et al: Infrared Physics & Technology 39 (1998)124.
2. J.W. Dees : Microware J. 9(1966) 48-55
3. L.O. Hocker, D. R. Sokoloff, V. Daneu, A. Szoke, A. Javan: Appl. Phys. Lett. 12 (1968) 401-402
4. S. M. Faris, T. K. Gustafson, J. C. Wiesner: IEEE J. Quantum. Electron. QE-9 (1963) 737-745
5. H.U. Daniel, M. Steiner, H. Walther: Appl. Phys. 25 (1981) 7-12
6. M. Heiblum, S. Wang, J. R. Whinnery, T. K. Gustafson: IEEE J. Quantum Electron. QE-14 159 (1978)
7. I. Wilke, W. Herrmann, F. K. Kneubuhl: Appl. Phys. B 58 (1994) 87-95
8. I. Wilke, Y. Oppliger, W. Herrmann, F. K. Kneubuhl: Appl. Phys. A 58 (1994) 329-341
9. C. Fumeaux, W. Herrmann, F. K. Kneubuhl, H. Rothuizen: Infared Physics & Technology 39 (1998) 123-182
10. G. L. Snider, A. O. Orlov, I. Amlani, X. Zuo, G. H. Bernstein, C. S. lent, J. R. Merz, and W. Porod, J. Vac. Sci. Technol. A 17 (4), 1999
11. Paul W. Kruse, Uncooled Thermal Imaging: Arrays, Systems, and Applications, Tutorial Texts in Optical Engineering, Vol. TT51, SPIE Pres, 2002.
12. A. M. Cowley and H. O. Sorensen, "Quantitative Comparison of Solid-State Microwave Detectors," IEEE Trans. Microwave Theory and Techniques, vol. 14, no. 12, pp. 588-602, 1966.
13. I. Bahl and P. Bhartia, Microwave Solid State Circuit Design, chapter 11, John Wiley & Sons, New York, 1988.
14. Aldert van der Ziel, Noise in Solid State Devices and Circuits, John Wiley & Sons, New York, 1986.